Hydrology and
Earth System
Sciences

Monitoring hillslope moisture dynamics with surface ERT for enhancing spatial significance of hydrometric point measurements

R. Hübner[1], K. Heller[1], T. Günther[2], and A. Kleber[1]

[1]Institute of Geography, Dresden University of Technology, Helmholtzstr. 10, 01069 Dresden, Germany
[2]Leibniz Institute for Applied Geophysics (LIAG), Stilleweg 2, 30655 Hanover, Germany

Correspondence to: R. Hübner (rico.huebner@tu-dresden.de)

Abstract. Besides floodplains, hillslopes are basic units that mainly control water movement and flow pathways within catchments of subdued mountain ranges. The structure of their shallow subsurface affects water balance, e.g. infiltration, retention, and runoff. Nevertheless, there is still a gap in the knowledge of the hydrological dynamics on hillslopes, notably due to the lack of generalization and transferability. This study presents a robust multi-method framework of electrical resistivity tomography (ERT) in addition to hydrometric point measurements, transferring hydrometric data into higher spatial scales to obtain additional patterns of distribution and dynamics of soil moisture on a hillslope. A geoelectrical monitoring in a small catchment in the eastern Ore Mountains was carried out at weekly intervals from May to December 2008 to image seasonal moisture dynamics on the hillslope scale. To link water content and electrical resistivity, the parameters of Archie's law were determined using different core samples. To optimize inversion parameters and methods, the derived spatial and temporal water content distribution was compared to tensiometer data. The results from ERT measurements show a strong correlation with the hydrometric data. The response is congruent to the soil tension data. Water content calculated from the ERT profile shows similar variations as that of water content from soil moisture sensors. Consequently, soil moisture dynamics on the hillslope scale may be determined not only by expensive invasive punctual hydrometric measurements, but also by minimally invasive time-lapse ERT, provided that pedo-/petrophysical relationships are known. Since ERT integrates larger spatial scales, a combination with hydrometric point measurements improves the understanding of the ongoing hydrological processes and better suits identification of heterogeneities.

1 Introduction

The knowledge of system-internal water flow pathways and the response to precipitation on different spatial and temporal scales is essential for the prediction of hydrological and hydrochemical dynamics within catchments (Uhlenbrook et al., 2008; Wenninger et al., 2004). Understanding the processes involved is of particular importance for improving precipitation-runoff and pollutant-transport models (Di Baldassarre and Uhlenbrook, 2012).

Hillslopes are important links between the atmosphere and the water input into catchments. They mainly control different runoff components and residence times (Uhlenbrook et al., 2008). Several studies have addressed hillslope hydrology (Anderson and Burt, 1990; Kirkby, 1980; Kleber and Schellenberger, 1998; McDonnell et al., 2001; Tromp-van Meerveld, 2004; Uchida et al., 2006). A major problem is that the spatial and temporal variability of the hydrological response due to different natural settings – e.g. geomorphological, pedological, lithological characteristics and the spatial heterogeneity – make it difficult to generalize and to transfer results to ungauged basins (McDonnell et al., 2007).

In catchments of Central European subdued mountain ranges, the shallow subsurface of hillslopes is mostly covered by Pleistocene periglacial slope deposits (Kleber and Terhorst, 2013). These slope deposits have developed in different layers. In the literature normally three layers are classified (upper layer – LH, intermediate layer – LM, basal layer – LB: classification according to AD-hoc AG-Boden, 2005; Kleber and Terhorst, 2013). Sometimes locally a fourth layer (*Oberlage* AD-hoc AG-Boden, 2005) could be found. The occurrence of these layers can vary spatially and has different

regional and local characteristics. Due to the sedimentological and substrate-specific properties, e.g. grain-size distribution, clast content and texture, they remarkably influence near-surface water balance (e.g. infiltration, percolation) and are of particular importance for near-surface runoff, e.g. interflow (Chifflard et al., 2008; Kleber, 2004; Kleber and Schellenberger, 1998; Sauer et al., 2001; Scholten, 1999; Völkel et al., 2002a, b; Heller, 2012; Moldenhauer et al., 2013).

Most of the prior studies were based on invasive and extensive hydrometric point measurements or on tracer investigations. Punctual hydrometric measurements may modify flow pathways and are not sufficient in the case of significant spatial heterogeneities in the subsurface. Tracer experiments, e.g. using isotopes, integrate much larger scales up to entire catchments but provide less direct insights into ongoing processes. Internal hydrological processes may be complex and due to the spatio-temporal interlinking of near-surface processes and groundwater dynamics, there is still a lack of knowledge regarding runoff generation in watersheds (McDonnell, 2003; Tilch et al., 2006; Uhlenbrook, 2005). For an efficient and accurate modelling of the hydrological behaviour at the crucial hillslope scale, additional methods are needed especially to improve the understanding of these complex processes in order to enhance the model hypotheses. Hydrogeophysical methods are capable of closing the gap between large-scale depth-limited remote-sensing methods and invasive punctual hydrometric arrays (Robinson et al., 2008a, b; Lesmes and Friedman, 2006; Uhlenbrook et al., 2008).

Many studies show the potential of electrical resistivity tomography (ERT) for hydrological investigation by means of synthetic case studies for aquifer transport characterization (Kemna et al., 2004; Vanderborght et al., 2005), imaging water flow on soil cores (Bechtold et al., 2012; Binley et al., 1996a, b; Garré et al., 2010, 2011; Koestel et al., 2008, 2009a, b), cross-borehole imaging of tracers (Daily et al., 1992; Oldenborger et al., 2007; Ramirez et al., 1993; Singha and Gorelick, 2005; Slater et al., 2000), or imaging of tracer injection or irrigation with surface ERT (Cassiani et al., 2006; De Morais et al., 2008; Descloitres et al., 2008a; Michot et al., 2003; Perri et al., 2012). However, some research has been conducted under natural conditions to characterize water content change, infiltration or discharge by use of cross-borehole ERT (French and Binley, 2004), surface ERT (Brunet et al., 2010; Benderitter and Schott, 1999; Descloitres et al., 2008b; Massuel et al., 2006; Miller et al., 2008) or a combined surface cross-borehole ERT array (Beff et al., 2013; Zhou et al., 2001).

Besides hydrogeophysical methods such as electromagnetics (EM) (Popp et al., 2013; Robinson et al., 2012; Tromp-van Meerveld and McDonnell, 2009), time-lapse ERT have been frequently applied to hillslope investigation in the runoff and interflow (Uhlenbrook et al., 2008; Cassiani et al., 2009) or preferential flow context (Leslie and Heinse, 2013).

However, the use of ERT for monitoring hydrological dynamics on hillslopes with layered structure is still rare.

The objective of this paper is to show the potential of minimally invasive surface time-lapse ERT as a robust methodological framework for monitoring long-term changes in soil moisture and to improve the spatial resolution of punctual hydrometric measurements (e.g. tensiometer and soil moisture sensors) on a hillslope with periglacial cover beds. Furthermore, we want to show the ability of ERT for mapping spatially heterogeneous structures and water content distributions of the shallow subsurface. With a multi-method approach, we attempt to demonstrate the possibility to adequately transfer hydrometric data to higher spatial scales and to obtain additional patterns of soil water dynamics on a hillslope. These scales are fundamental for achieving a better understanding of the influence of the layered subsurface on water fluxes (e.g. infiltration, percolation or interflow) and the response to different amounts of precipitation on hillslopes.

2 Material and methods

2.1 Study site

The study area covers 6 ha of a forested spring catchment in the Eastern Ore Mountains, eastern Germany, which is located in the Freiberger Mulde catchment (Fig. 1).

Annual precipitation averages 930 mm, mean annual temperature is 6.6 °C. The altitude ranges from 521 to 575 m a.s.l. with a predominant land cover of spruce forest (*Picea abies*, approx. 30 years). The slope angle of the catchment ranges from 0.05 to 22.5° with an average of 7°. Bedrock is gneiss overlain by periglacial cover beds with up to three layers (LH, LM, LB, with no occurrence of the *Oberlage*, see Heller, 2012). The upper layer (LH) with a thickness of 0.3–0.65 m consists of silty–loamy material with a bulk density of $1.2 \, \text{g m}^{-3}$ and many roots (see Table 1). In the central part of the catchment, a silty–loamy intermediate layer (LM) follows with higher bulk density and a thickness of up to 0.55 m. The ubiquitous sandy–loamy basal layer (LB) is characterized by even higher bulk density and longitudinal axes of coarse clasts oriented parallel to the slope. Downslope it may reach a thickness of at least 3 m (see Fig. 1).

2.2 Laboratory work

Quality, amount and distribution of pore water exert a huge influence on resistivity [1] and form the link between electrical and hydrological properties. The empirical relationship of Archie's law (Archie, 1942) describes the connection between electrical resistivity and saturation in porous media.

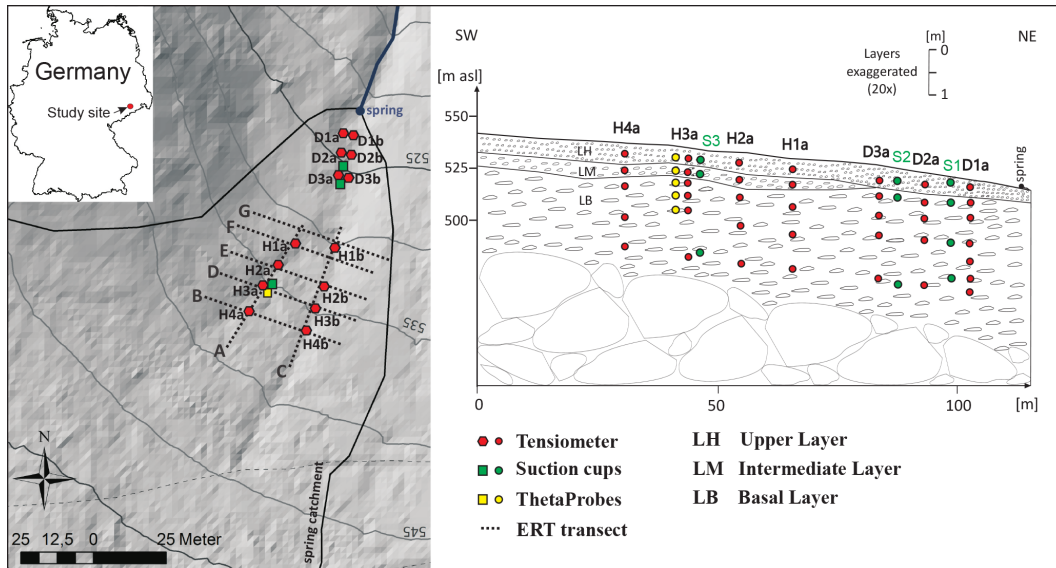[1]In this context the term "resistivity" always refers to " specific electrical resistivity".

Figure 1. Study site with locations of ERT profiles and hydrometric stations (left panel; data source: ATKIS®-DGM2, Landesvermessungsamt Sachsen, 2008) and profile section with installation depths of tensiometers, soil moisture sensors and suction cups (right panel).

Table 1. Properties of cover beds from the study site ($n \geq 15$ per layer) – adapted from Moldenhauer et al. (2013).

| Layer | Soil horizon | Colour (moist) | Soil texture | | | | Bulk density ($g\,m^{-3}$) | Porosity | Hydraulic conductivity ($cm\,d^{-1}$)* |
			Clay (%)	Silt (%)	Sand (%)	Clasts (%)			
LH	A/Bw	10YR/5/8	14	52	34	36	1.2	0.55	27
LM	2Bg	10YR/5/4	12	53	35	43	1.5	0.43	9
LB	3CBg	10YR/5/3	7	22	71	56	1.7	0.36	52

* Field-saturated hydraulic conductivity measured using the compact constant head permeameter (CCHP) method (Amoozegar, 1989).

Instead of saturation we use the volumetric water content θ with

$$\rho_{\text{eff}} = F_\theta \rho_{\text{w}} \theta^{-n_\theta}, \qquad (1)$$

where ρ_{eff} is the bulk resistivity of the soil probe and ρ_{w} is the resistivity of the pore fluid. The formation factor F_θ describes the increase of resistivity due to an insulating solid matrix and constitutes an intrinsic measure of material microgeometry (Schön, 2004; Lesmes and Friedman, 2006). The exponent n_θ is an empirical constant, which depends on the distribution of water within the pore space (Schön, 2004).

This model disregards the surface conductivity, which may occur due to interactions between pore water and soil matrix, especially with a high percentage of small grain sizes. In our study the curve fitting could be carried out very well without accounting for surface conductivity.

To investigate the pedo-/petrophysical relationship between resistivity and water content, 14 undisturbed soil core specimens (diameter = 36 mm, length = 40 mm) taken at different depths (0.3–1.4 m) were analysed. After dehydration in a drying chamber, the samples were saturated. The satura-

tion was done successively by stepwise injection in the middle of the soil core to achieve a better moisture distribution within the sample. Using a four-point array, electrical resistivity was measured for different saturation conditions during the saturation process. A calibrating solution with known resistivity was used to determine the geometric factor. Particle sizes were determined by sieving and the pipette method, using $Na_4P_2O_7$ as a dispersant (Klute, 1986, p. 393, 399–404, but with the sand–silt boundary at 0.063 mm).

Brunet et al. (2010) described remarkable conductivity increases of low mineralized water due to contact with the soil matrix. This may cause variation of resistivity with time. To minimize this effect we used spring water with high conductivity (approx. $\sigma_{\text{w25}} = 150\,\mu S\,cm^{-1}$ / $\rho_{\text{w25}} = 66\,\Omega\,m$ for $T = 25\,°C$). This corresponds to the mean conductivity of soil water in the study area, which is influenced by long-term contact with the subsoil.

Aside from the invariant parameters F_θ and n_θ, the resistivity of the pore water must be known to calculate the water content from resistivity values. Because it was not possible to extract pore water under dry conditions in summer, only

Table 2. Median pore water conductivity $\tilde{\sigma}_w$, resistivity $\tilde{\rho}_w$ and mean resistivity $\bar{\rho}_w$ with standard deviation (SD$_w$) per depth ($n \geq 11$ per sampling depth).

Depth [m]	0.3	0.6	0.85	1.05	1.65	2.3
$\tilde{\sigma}_w$ [µS cm^{-1}]	72.4	107.8	111.6	114.7	135	156.7
$\tilde{\rho}_w$ [Ω m]	138.1	92.8	89.6	87.2	74.1	63.8
$\bar{\rho}_w$ [Ω m]	135.7	92.3	88.9	86.8	75.1	63.7
SD$_w$ [Ω m]	16.9	5.0	4.5	4.8	5.4	7.3

a few measurements of pore water conductivity could be carried out in late spring and early autumn. To calculate water content from resistivity obtained by field surveys, the median value over the entire time period of ρ_w for each depth was used (see Table 2). Interim values between the extraction depths were linearly interpolated.

After reforming Eq. (1) it is possible, with known parameters F_θ and n_θ and measured variables ρ_{eff} and ρ_w, to calculate volumetric water content:

$$\frac{\rho_{eff}}{F_\theta \rho_w}^{\frac{1}{-n_\theta}} = \theta. \quad (2)$$

As water saturation (S) is defined as the ratio between water content and porosity (Φ), it is also possible to calculate the degree of saturation using

$$\frac{\rho_{eff}}{F_\theta \rho_w}^{\frac{1}{-n_\theta}} \frac{1}{\Phi} = S. \quad (3)$$

The porosity (Φ) was calculated with

$$\Phi = 1 - \frac{\rho_{bulk}}{\rho_{particle}}. \quad (4)$$

The bulk density (ρ_{bulk}) was determined using undisturbed core samples. The particle density ($\rho_{particle}$) was measured with a capillary-stoppered pycnometer. The maximum sample depth for undisturbed soil cores was < 2 m. Below, the porosity had to be transferred according to grain size distribution, clasts and compaction from percussion drilling.

2.3 Field work

2.3.1 ERT mapping

In addition to conventional percussion drilling, at the end of October 2008 we measured seven ERT profiles to survey the subsurface resistivity distribution (A–G in Fig. 1). A and C are parallel to the slope inclination of approx. 9°, connecting inflection points of contour lines. B, D, E, F and G are perpendicular to these profiles ($\angle$ A102.5°, $\angle$ C90°). This arrangement allows identifying potential 3-D effects, which may cause inaccurate interpretation of the subsurface resistivity distribution. To improve the mapping results aided by hydrometric data, the profiles were located close to the tensiometer stations (distance < 2 m). For all resistivity measurements, the instrument "4 Point light hp" from "LGM –

Lippmann Geophysical Equipment" with 50 electrodes was used. Because of the expected interferences (e.g. by roots or clasts) and the multiple-layered stratification of periglacial cover beds, a Wenner array was found to be the most suitable configuration for the study area. This is characterized by low geometric factors (K), a high vertical resolution for laterally bedded subsurface structures, and a good signal-to-noise ratio (Dahlin and Zhou, 2004). To improve the spatial resolution, a Wenner-β array was measured additionally. With an electrode spacing of 1 m, this results in a combined data set with 784 data points for each pseudo-section with a maximum depth of investigation of 9.36 m (Wenner-β: depth of investigation for radial dipole in homogeneous ground $0.195L$ with L the maximum electrode separation in metres, according to Roy and Apparao, 1971; Apparao, 1991; Barker, 1989).

Horizontal resolution of a multi-electrode array is for shallow parts of the subsurface of the order of electrode distances. However, vertical resolution is far better, as the depth-of-investigation curves indicate (Roy and Apparao, 1971; Barker, 1989). This is further improved by measuring two electrode arrays (Wenner and Wenner-β) with different sensitivity curves so that we can expect a vertical resolution of the order of about 0.2 m in the case of excellent data quality.

2.3.2 Joint hydrometric and ERT monitoring

Since November 2007 soil water tension has been measured using 76 recording tensiometers (T8, UMS) arranged in 14 survey points along the slope at 5–7 different depths (see Fig. 1). Additionally, at the survey point H3a five soil moisture sensors (ThetaProbe, ML2x, Delta-T) were installed to measure volumetric water content. A V-notch weir with a pressure meter was used to quantify spring discharge. Rainfall was recorded by four precipitation gauges with tipping bucket (R. M. Young Co., 200 cm^2, resolution: 0.1 mm with max. 7 mm min^{-1}). For determination of pore water conductivity and resistivity, soil water was extracted with suction cups (VS-pro, UMS) at four depths at three locations (S1, S2, S3; Fig. 1) and cumulated as a weekly mixed sample.

Time lapse ERT measurements were performed with the same equipment, electrode array and spacing used for the mapping. The two time lapse profiles are congruent with profiles A and B (see Fig. 1). From May to December 2008, twenty seven time lapse measurements were carried out within almost weekly intervals. Contact resistance was checked before each measurement and was within the range of 0.2 kΩ to max. 1 kΩ over the whole measuring period. This range is very favourable and does not influence the measurements as numerical studies show (Rücker and Günther, 2011).

To compare time lapse measurements and to apply sophisticated inversion routines, the location of electrodes needs to remain constant. For current injection we used stainless steel electrodes (diameter 6 mm, length 150 mm), completely

plunged into the ground, thus avoiding shifting of electrodes, except for natural soil creep. In the numerical computations, electrodes are considered points, which is not the case for the present ratio of length to distance. However, numerical computations with real electrode lengths show that the deviations are negligible, particularly if the points are placed at about half the electrode length (Rücker and Günther, 2011).

Subsoil temperature, especially in the upper layers, is characterized by distinct annual and daily variations. Therefore, the temperature dependence of resistivity must be considered when comparing different time steps. The installed tensiometers are able to measure soil temperature simultaneously. These data have been used to correct resistivity measurements to a standard temperature. Comparing several existing models for the correction of soil electrical conductivity measurements, Ma et al. (2011) conclude that the model (Eq. 5) proposed by Keller and Frischknecht (1966) is practicable within the temperature range of environmental monitoring:

$$\rho_{25} = \rho_t \left(1 + \delta \left(T - 25\,^\circ\text{C}\right)\right). \tag{5}$$

With this equation the inverted resistivity (ρ_t) at the temperature (T) was corrected to a resistivity at a soil temperature of $25\,^\circ\text{C}$ (ρ_{25}). The empirical parameter δ is the temperature slope compensation, with $\delta = 0.025\,^\circ\text{C}^{-1}$ being commonly used for geophysical applications (Keller and Frischknecht, 1966; Hayashi, 2004; Ma et al., 2011).

2.3.3 ERT data inversion

For inversion of the ERT data, we used the BERT Code (Günther et al., 2006). In order to account for the present topography, we used an unstructured triangular discretization of the subsurface and applied finite element forward calculations. For static inversion, a smoothness-constraint objective function is minimized that consists of the error-weighted misfit between measured data $\mathbf{d}$ and model response $\mathbf{f(m)}$, and a model roughness:

$$\Phi = \|\mathbf{D}(\mathbf{d} - \mathbf{f(m)})\|_2^2 + \lambda \|\mathbf{Cm}\|_2^2 \to \min. \tag{6}$$

The regularization parameter λ defines the strength of regularization imposed by the smoothness matrix $\mathbf{C}$ and needs to be chosen such that the data are fitted within expected accuracy, which is incorporated in the data weighting matrix $\mathbf{D}$. In our case, values of $\lambda = 30$ provided sufficient data fit. See Günther et al. (2006) for details of the minimization procedure, and Beff et al. (2013) or Bechtold et al. (2012) for specific modifications in hydrological applications.

For time lapse inversion, i.e. calculating the temporal changes in resistivity, there are three different methodical approaches: (i) inverting the models for each point in time separately, (ii) using the initial model as reference model for the time step, (iii) or inverting the differences of the two data sets (Miller et al., 2008). With our data, each method generates insufficient results with unsubstantiated artifacts. An

increase on the surface was always followed by a decrease below and vice versa. These systematic changes cannot be explained or related to any natural process. Descloitres et al. (2003, 2008b) showed with synthetic data that time lapse inversion may produce artifacts due to the smoothness constraints especially with changes caused by shallow infiltration (decrease of resistivity), as mostly expected in our case.

As smoothness constraints are the main reason of these problems, we avoid the smoothness operator in the time lapse inversion and minimize a different objective function for the subsequent time steps:

$$\Phi = \|\mathbf{D}(\mathbf{d}^n - \mathbf{f}(\mathbf{m}^n))\|_2^2 + \lambda \|\mathbf{m}^n - \mathbf{m}^{n-1}\|_2^2 \to \min. \tag{7}$$

Beginning from the static inversion, the subsequent models are found by reference model inversion. Only the total difference between the models of subsequent time steps $n-1$ and n is used for regularization (minimum-length constraints). A higher regularization parameter of $\lambda = 100$ proved optimal for time lapse inversion concerning both data fit and in comparison to the hydrometric results.

In order to find representative resistivity values as a function of depth, which are independent on small-scale heterogeneities, we subdivide the model down to a depth of 3 m into seven layers according to the boundaries of the described layering (see Table 1) and installation depth of hydrometric devices (see Fig. 1) (0–0.2, 0.2–0.4, 0.4–0.9, 0.9–1.2, 1.2–1.5, 1.5–2.0 and 2.0–3.0 m). The representative values are median resistivities in the layers from the stations H1a–H4a and H4b–H4a for profiles A and B, respectively.

3 Results

3.1 Laboratory

Within the separately analysed samples, non-linear curve fitting was carried out. Using the method of least squares, the data could be fitted using a power function in the form of Archie's law (Eq. 1, $0.973 < r < 0.999$).

The exponent n_θ shows a positive correlation to small grain sizes, primarily medium silt (6.3–20 µm, $r = 0.909$), but in the same case a negative correlation to grain sizes > 630 µm including clast content ($r = -0.852$) (see Fig. 2).

The amount of silt as well as the clast content are important distinctive attributes to differentiate the basal layer from the overlying intermediate or upper layer (Table 1). Two different "electrical" layers may be identified. This is due to the fact that the exponent is strongly influenced by grain size, which shows a remarkable change at the upper boundary of LB. On the other hand, grain size distribution and clast content are very similar between LH and LM, so that these may not be differentiated using ERT. Figure 3 shows the aggregation of the 14 single samples into two regions with different depth ranges.
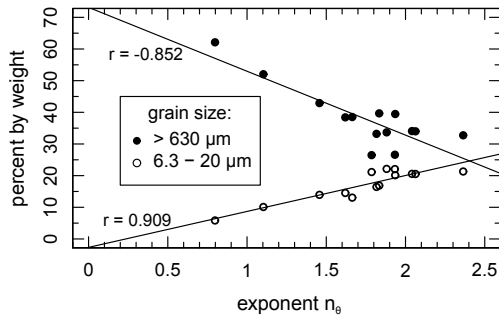
Figure 2. Exponent n_θ in dependence of different grain sizes.

Figure 3. Volumetric water content in dependence of resistivity ratio ($\rho_{\text{eff}}/\rho_{\text{w}}$) for two different depth ranges.

Table 3. Fitted water content formation factor (F_θ), water content exponent (n_θ) and mean squared error for $\rho_{\text{eff}}/\rho_{\text{w}}$ (MSE) for Eqs. (1)–(3) of the two different depth ranges.

Depth range	F_θ	n_θ	r^*	MSE
$< 0.9\,\text{m}$	0.577	1.83	0.895	2.8
$\geq 0.9\,\text{m}$	0.587	1.34	0.888	1.4

$^*\ p < 0.01.$

The first depth range comprises the upper and the intermediate layer. These two periglacial layers are characterized by a high amount of silt (mostly medium silt) and comparatively low clast content. The exponent n_θ ranges from 1.8 to 2.3. The second depth range is represented by the basal layer. This is characterized by a higher amount of coarse material at the expense of fine grain sizes. In this depth range n_θ ranges from 0.7 to 1.8. Within each of these two depth ranges, we assume, analogously to the properties of the substrate, similar electrical properties with a threshold at 0.9 m. The threshold depth of 0.9 m is not developed as an exact, continuous boundary. Rather it is a short transition zone, because the samples right from this depth may have properties of the shallow or the deeper region, similar to the geomorphological differentiation between the basal and intermediate layer, whose boundary varies between depths of 0.8 to 1 m. By combining samples from different depths into two regions, it was possible to derive the parameter for Eqs. (1)–(3) for each region (Table 3).

This relationship between water content and resistivity, shown in Fig. 3 and Table 3, is only a mean value for each depth range. In the first depth range (0–0.9 m), especially close to the surface, the differences in soil or electrical properties between the samples even at the same depth may vary. This higher variation may be explained by intense biotic activity near the surface, enhancing small-scale heterogeneity compared to deeper parts of the soil.

The fitted curves of both regions are quite similar, except for n_θ. The adapted values for F_θ are almost identical (0.577 vs. 0.587, Table 3). With high saturation, the difference of resistivity between the depth ranges is small and

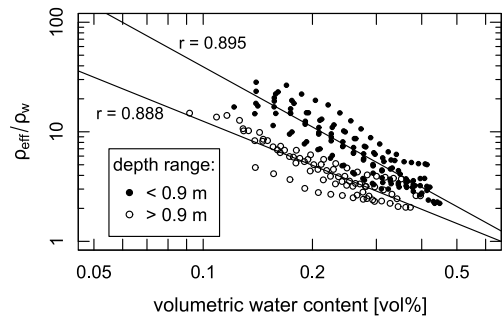primarily influenced by the conductivity of the pore fluid, but increases with decreasing water content. As a result of the higher exponent, LH and LM react more sensitively to water content changes than LB, especially at low presaturations. Related to this, small water content changes cause larger changes in resistivity than in the deeper region.

3.2 ERT mapping

At our study site the resistivity of the subsoil ranges from nearly 100 Ω m up to more than 4000 Ω m. The distribution may be divided in two main areas, the "inner" area between the depression lines and the "outer" area at the hillsides which differ in their depth profiles. (see Fig. 4)

At the intersection between the longitudinal and diagonal profiles, a good match of the calculated resistivity models can be found at shallow depth. With increasing depth, the differences become more notable – e.g. A × B: depth < 1 m, average deviation 8 % ($\sigma = 5.4$ %); depth 1–7 m, average deviation 20 % ($\sigma = 10$ %); and depth > 7 m, average deviation 43 % ($\sigma = 6.6$ %). To exclude potential errors (e.g. electrode positioning errors), the data quality may be evaluated by comparing normal and reciprocal measurements, i.e. interchanging potential and current electrodes (LaBrecque et al., 1996; Zhou and Dahlin, 2003). For profiles A and B repeated measurements with reciprocal electrode configuration were conducted. Thereby, no large errors (max ±1.2 %) could be found between normal and reciprocal measurements. Because of the absence of large potential errors, the increasing deviation with depth may be only explained by the inversion process, decreasing sensitivity, less spatial resolution or potential 3-D effects.

The resistivity distribution of the subsurface is characterized by large-scale and small-scale heterogeneities, but also distinct patterns may be identified. At shallow depth up to 0.9 m, the study area is characterized by high resistivity. This comprises the upper and the intermediate layer.

Since the laboratory results indicate similar electrical properties, remarkable differences between upper and intermediate layers only occur if water content deviates. There
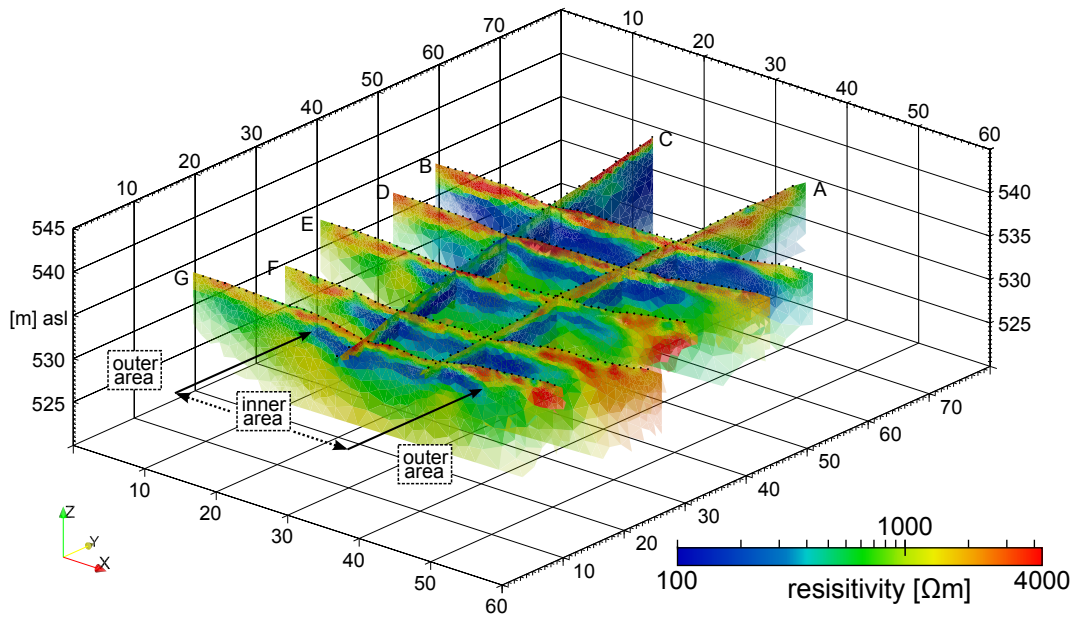
Figure 4. Resistivity results from ERT mapping (October 2008) of the study area: pseudo 3-D view of the profiles A to G.
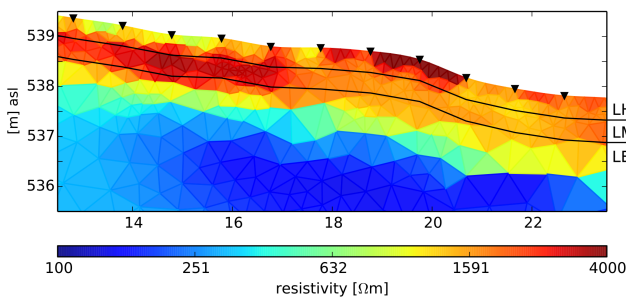

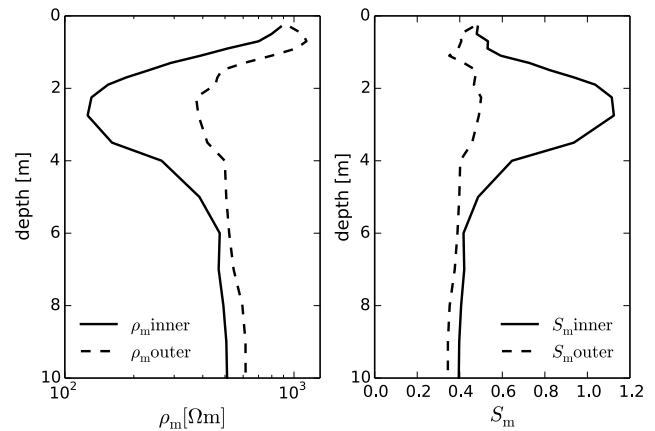**Figure 5.** ERT section of profile A with plotted layer boundaries (date: 21 October 2008).

are areas where the intermediate layer has higher resistivity, suggesting lower water content (see Fig. 5).

The hydrometric data show the driest conditions in 0.55–0.65 m (see Fig. 8) which is consistent with the high median resistivity of the intermediate layer at the time of data acquisition (see Fig. 6).

Resistivity decreases in greater depths (starting at 1 m). Thus, the basal layer is characterized by lower resistivity compared to the overlying layers. However, this is not constant in the lateral direction. Two different patterns are found. In the "inner" area between the two depression lines (approx. between profiles A and C), the resistivity of the basal layer is lower than in the "outer" area (the hillsides) (see Fig. 6). Between the depression lines LB is characterized as a connected zone of low resistivity. A calculation of saturation using Eq. (3) and the porosity from Table 1 indicates that this may be interpreted as a connected saturated zone (Fig. 6).

Figure 6. Median resistivity (left panel) and median water saturation (right panel) per depth for the inner region (between the depression lines) and outer region (hillslopes) (date: 21 October 2008).

Due to the slope gradient, water from the hillsides and upper parts of the catchment flows into the direction of the depression lines, where it concentrates and forms a local slope groundwater reservoir. This results in a maximum decrease of resistivity in this zone as observed in all measured profiles at depths of 1.5–4.5 m (see Figs. 4 and 6). Percussion drilling confirmed that the thickness of LB exceeds 3.5 m downslope. Therefore, we assume that the entire saturated zone is located within the basal layer and since it is connected to the spring, it is also the source of the base flow. According to this, the shape of the surface may be partially transferred to the subsurface to identify regions of different hydrogeological conditions. Convex areas indicate dryer conditions in
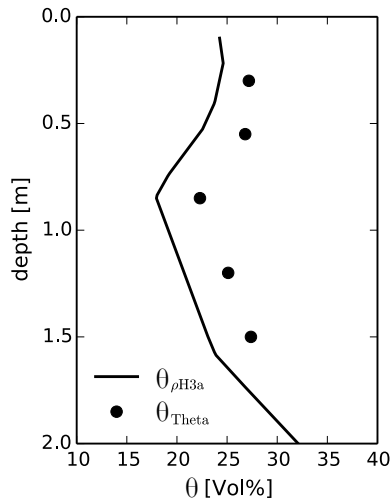
Figure 7. Volumetric water content calculated from resistivity data close to H3a in comparison with soil moisture sensors (date: 21 October 2008).

3.3 Joint hydrometric and ERT monitoring

During the period May to December 2008 the spring discharge varied between 0.07 and $1.67\,\mathrm{L\,s^{-1}}$. Median soil water tension of the study area, related to depth and time (see Fig. 8), indicates the impact of soil moisture on spring discharge. During summer increasing evapotranspiration causes the drying-out of soil. The spring showed only a slight reaction to precipitation events. Rainfall could only balance the soil water deficit and caused no runoff. Therefore, there is almost no runoff generation in the summer season. Primarily base flow dominates and decreasing discharge is mainly caused by saturation excess overland flow from the area surrounding the spring.

In contrast, during winter season (starting in November) at all depths lower tensions ($< 90\,\mathrm{hPa}$) were measured. Less evapotranspiration results in a replenishment of the storage water reservoirs in the subsurface. Due to the moist conditions, high presaturations predominate and cause a rapid runoff response with rain and the high discharges within the winter season.

Furthermore, there is an influence of the layered subsurface on soil moisture and runoff response. Until the beginning of May and again from December the low tensions of the upper parts of LB indicate saturated conditions, in contrast to the deeper LB with higher tensions (see Fig. 8). Due to the anisotropic hydraulic properties (low vertical compared to horizontal hydraulic conductivity) the percolation into deeper parts of LB decreases. The seepage water is concentrated as backwater in the LM and the upper parts of LB. Because of the high lateral hydraulic conductivity this saturated depth range is mainly involved in runoff and causes strong interflow.

As the hydrometric data show, the first period from May to October was mainly characterized by drying of the subsurface. After that, humid conditions began to dominate (see Fig. 8). Major changes occur at shallow depth and proceed to depth, though remarkably attenuated. Each depth has its own characteristics, its own variation in time and shows different hydrological and electrical response. To better distinguish the results and to deal with the subsurface layered structure, a depth- or layer-based analysis is appropriate.

Figure 9 shows the trend of median resistivity for each depth range for the entire time series of profile A between H1a and H4a and profile B between H4b and H4a, in comparison with daily accumulated precipitation.

The resistivity of profile A clearly correlates with profile B (Table 4). This correlation is more pronounced at shallow depths. The absolute values are similar, except for the near-surface part of LH (0–0.2 m) and parts of LB (1.5–2.0 m). These two depth ranges have higher resistivity values at profile B than A at all points in time, due to the different positions. Profile A is completely situated in one of the depression lines, in which higher soil water contents can be expected in general.
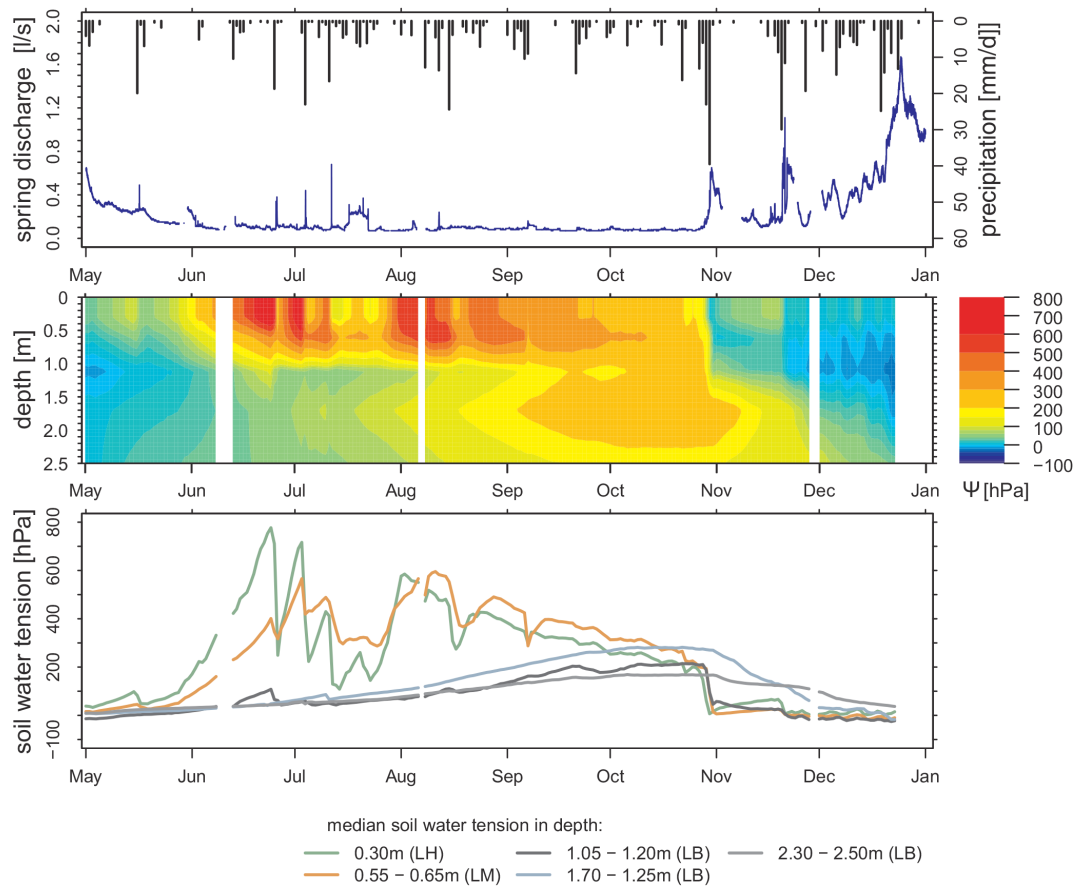
the basal layer in comparison to concave or elongated parts of the hillslope, which may act as local aquifers.

It is not feasible to relate a resistivity to the underlying gneiss or its regolith. Percussion drilling was only realized down to 4 m depth where bedrock could not be reached. If the maximum thickness of the basal layer is equal to the saturated zone, as obtained by resistivity data, the change from basal layer to underlying gneiss may be set at a depth around 4.5 m.

ERT mapping of the spatial distribution of periglacial cover beds is associated with several restrictions. In our study area, stratification is concealed by the influence of pore water, the main factor driving resistivity. On the other hand this fact may be used to improve the understanding of the moisture conditions of the subsurface.

To check the equations obtained in the lab and also to compare directly with hydrometric data, we used the water contents from the soil moisture sensors at H3a. Figure 7 compares water content, calculated with temperature-corrected resistivity ($\theta_{\rho H3a}$ profile A close to H3a), with water content from the ThetaProbes (θ_{Theta}) at time of mapping.

The values of $\theta_{\rho H3a}$ and θ_{Theta} show depth profiles of similar shape, but the values differ slightly. The resistivity depth profile shows a shift of -4.5 Vol% in comparison to the ThetaProbes. The different positions of the two probe locations could be one reason for this mismatch. Other reasons could be the inversion process of the resistivity data or differing pore water resistivity from the used median value (Table 2).

Because the data of the resistivity measurements and also the ThetaProbes may contain biased errors (e.g. caused by clast content or by the installation procedure), it is difficult to draw reliable conclusion as to which depth profile is more accurate.

Figure 8. Spring discharge in comparison with daily precipitation (top panel), image of median soil water tension of the shallow subsurface (middle panel) and median soil water tension for different depths (bottom panel) – adapted from Heller (2012).

Table 4. Correlation between median resistivity of profiles A ($\rho_{\text{profile A}}$) and B ($\rho_{\text{profile B}}$) and between subsequent resistivity ratio of profile A ($\rho_{\text{timestep}}/\rho_{\text{initial}}$) and cumulative precipitation during the time step (ppt).

Depth [m]	$r_{(\rho_{\text{profile A}}, \rho_{\text{profile B}})}$ [a]	$r\left(\frac{\rho_{\text{timestep}}}{\rho_{\text{initial}}}, \text{ppt}\right)$
0–0.2	0.977	-0.773[a]
0.2–0.4	0.988	-0.770[a]
0.4–0.9	0.987	-0.804[a]
0.9–1.2	0.987	-0.586[a]
1.2–1.5	0.852	-0.378[b]
1.5–2.0	0.831	-0.078[b]
2.0–3.0	0.878	0.173[b]

[a] $p < 0.01$; [b] $p > 0.01$.

During the measuring period, the upper layer (0–0.2 and 0.2–0.4 m) reacts with similar resistivity variations as the intermediate layer (0.4–0.9 m). Resistivity of the intermediate layer may temporarily exceed the upper layer (e.g. profile A, October–December).

The temporal changes in resistivity decrease with depth. Short time variations are limited down to 2 m. Below, the differences are marginal with only a continuous slight increase during the investigated period.

The variation of resistivity is significantly influenced by rainfall. As shown in Table 4, the upper and intermediate layers (< 0.9 m) show a strong negative correlation with the cumulated amount of precipitation (ppt). This correlation decreases with depth. Upper parts of the basal layer (0.9–1.5 m) respond slightly and with a delay to intense rain events or enduring dry periods. Depths > 1.5 m show no direct correlation with rainfall. Water cannot infiltrate straight to greater depths because of decreasing hydraulic conductivity, evaporation, storage, or consumption of water by roots.

One problem is the temporal resolution. Because of the time intervals (usually ≥ 1 week), we are not able to resolve the entire temporal heterogeneity of the subsurface, which may lead to misinterpretation. For example, during the period from 3 to 16 September, the amount of 33 mm rain seems not to affect the resistivity of profile A. However, 32 of these 33 mm had already been fallen by 7 September. At profile B with an additional measurement on 9 September, resistivity
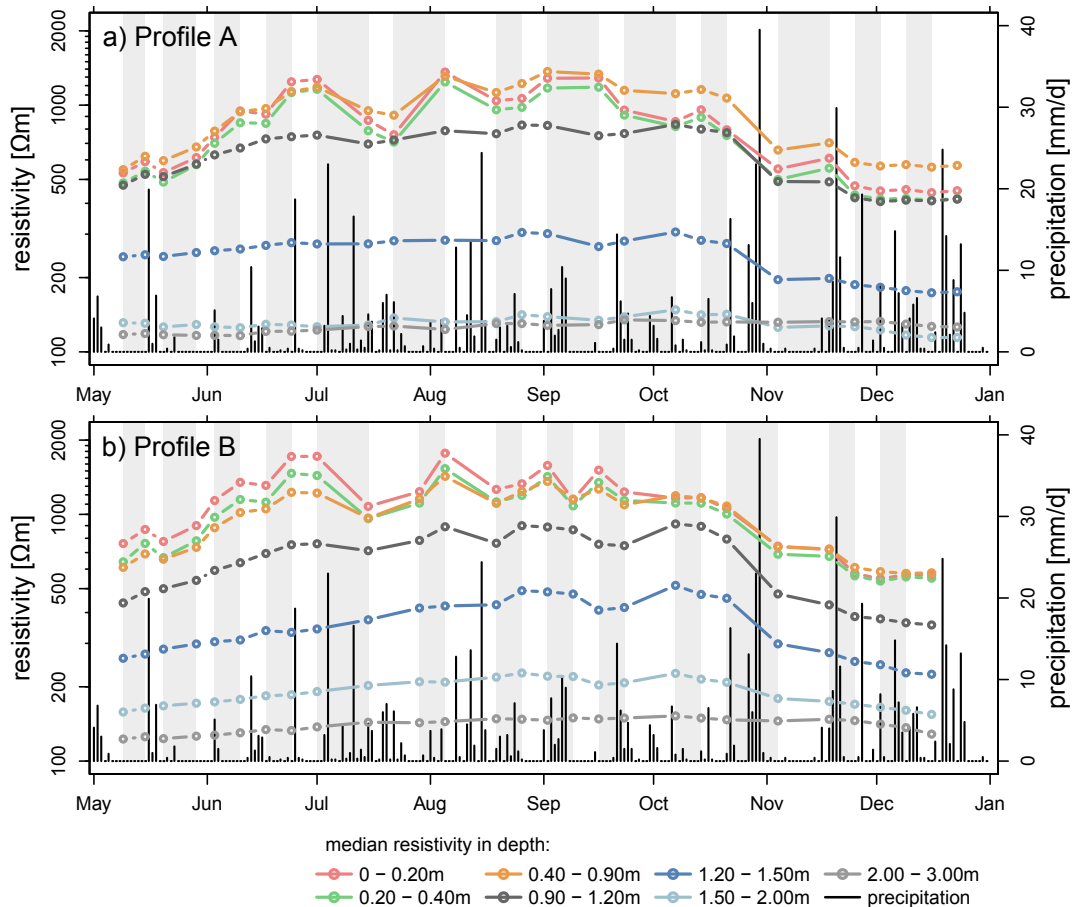
Figure 9. Trend of median resistivity for different depth ranges for **(a)** profile A and **(b)** profile B in comparison with daily precipitation (grey and white shaded regions for visualization of ERT time intervals).

at shallow depth decreases first and after that increases back to the initial level of 3 September (see Fig. 9b). Due to the missing time step, this alteration is not traced in profile A (see Fig. 9a).

This issue is also evident when comparing the resistivity with the soil suction data. With the higher temporal resolution of the tensiometer it is possible to resolve short time events, e.g. single rain events (Fig. 8), which cannot be rendered with the resistivity survey (see Fig. 9).

During the investigation period, different trends could be identified. The initial conditions in April and early May are characterized by a highly saturated subsurface. This is indicated by low soil water tension, high spring discharge and high water content. Due to the humid conditions at the beginning of the measurements, the conductivity of the shallow subsurface is high and the observed resistivity is low relative to the seasonal variations.

The first period between May and October is mainly characterized by increasing resistivity. The accumulated precipitation from 9 May to 21 October is only 337 mm. In combination with increasing evapotranspiration, this causes a drying

of the subsurface (see Fig. 8). As a result of drying, at shallow depths (< 0.9 m) resistivity quickly increases until July. Below, the increase proceeds slightly, but continuously until October.

As mentioned above, resistivity, especially of LH and LM (up to 0.9 m), shows a high short time variability and is strongly associated with the amount of precipitation (ppt) (Table 4). During the investigated period three different response types could be identified that are exemplarily illustrated in Fig. 10 and compared to soil water tension.

1. A small amount of precipitation (see 23 September–7 October, ppt = 23 mm) causes a short deferment of increasing resistivity of LH and LM during the summer period. The values of initial state and time step are of the same order of magnitude. Within the temporal resolution, only a slight decrease could be recorded. Deeper parts are not affected and dry continuously. Constant discharge indicates that there is no runoff generation during this period. This amount of rain is only able to balance the deficit caused by evaporation at shallow
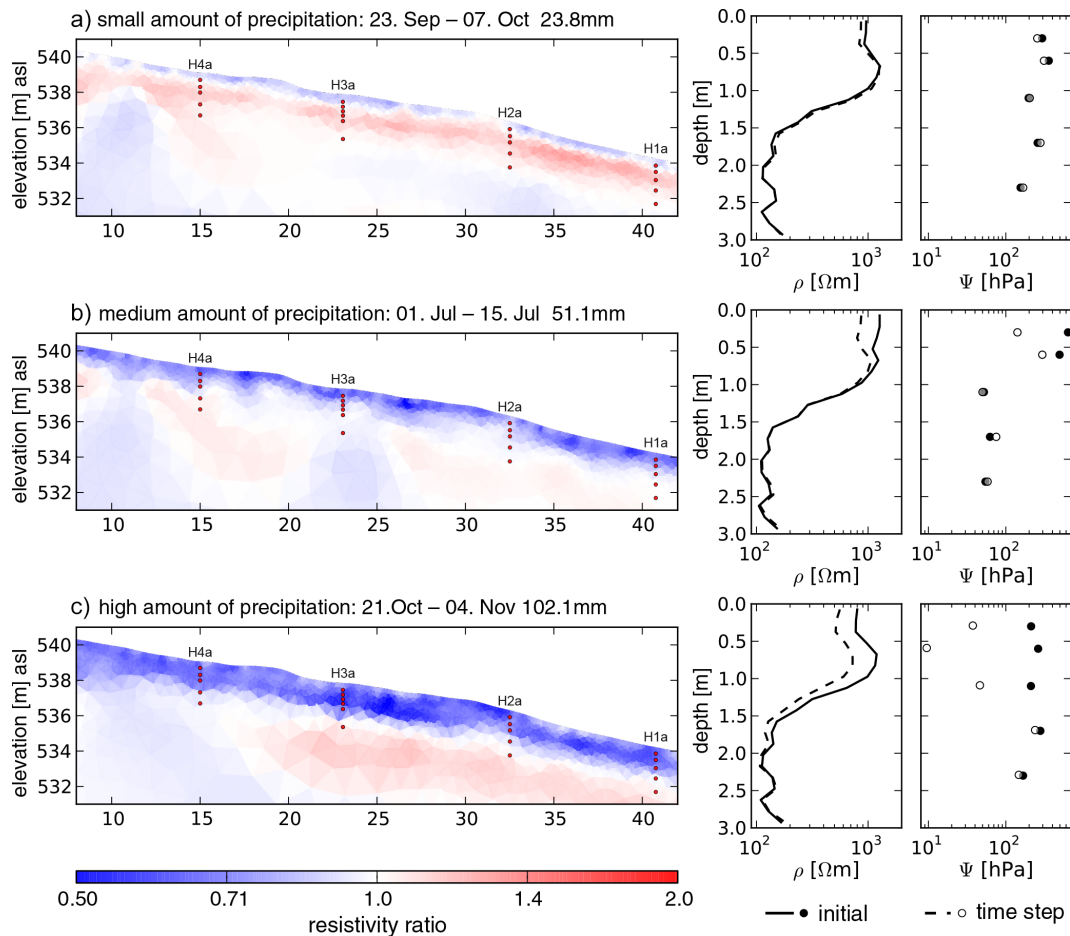
Figure 10. Ratio between subsequent resistivity (first column), median resistivity as a function of depth (second column) and median soil water tension (third column) for three exemplary precipitation responses: **(a)** small amount, **(b)** medium amount and **(c)** high amount.

depths, at least within the temporal resolution of measurements.

2. A medium amount of precipitation (see 1 July–15 July, ppt = 51.1 mm) causes a distinctive reaction at shallow depth. Resistivity at these depths shows a sharp decrease by comparatively the same ratio (~ 0.7). However, the signal is not traced into the deeper ground (> 1.2 m), which remains completely unaffected. So vertical seepage dominates in LH and LM, which leads to recharge of soil water. The water is predominantly fixed by capillary force; hence it does not percolate into deeper layers. The short rise of discharge is caused by saturation overland flow in the spring bog.

3. A high amount of precipitation (see 22 October–4 November, ppt = 102.1 mm) results in a strong response down to 2.0 m and affects LH, LM as well as parts of LB. Such a heavy rain period does not induce larger resistivity changes in LH and LM than the medium rain period, but influences deeper regions at the same order of magnitude as above. The water infiltrates to the

upper, but does not reach the deeper parts of the basal layer (2–3 m). The vertical seepage is limited and therefore the increasing spring discharge may only be caused by lateral subsurface flow, such as interflow in the unsaturated subsoil.

After the major rain event at the end of October, resistivity values remain constant until the next time step. Due to precipitation of 102.1 mm during the period from 19 November to 16 December, resistivity drops below the initial state and shows highly saturated conditions.

A comparison of water content obtained by soil moisture sensors (θ_{Theta}) and water content calculated from resistivity data for different depths over time at profile A close to the hydrometric station H3a ($\theta_{\rho\text{H3a}}$) using Eq. (2) is shown in Fig. 11

At shallow depth (≤ 0.85 m), $\theta_{\rho\text{H3a}}$ correlates closely with θ_{Theta} (Table 5). However, there is a shift of the curves during the whole period. The volumetric water content from resistivity data is consequently smaller than from the soil moisture
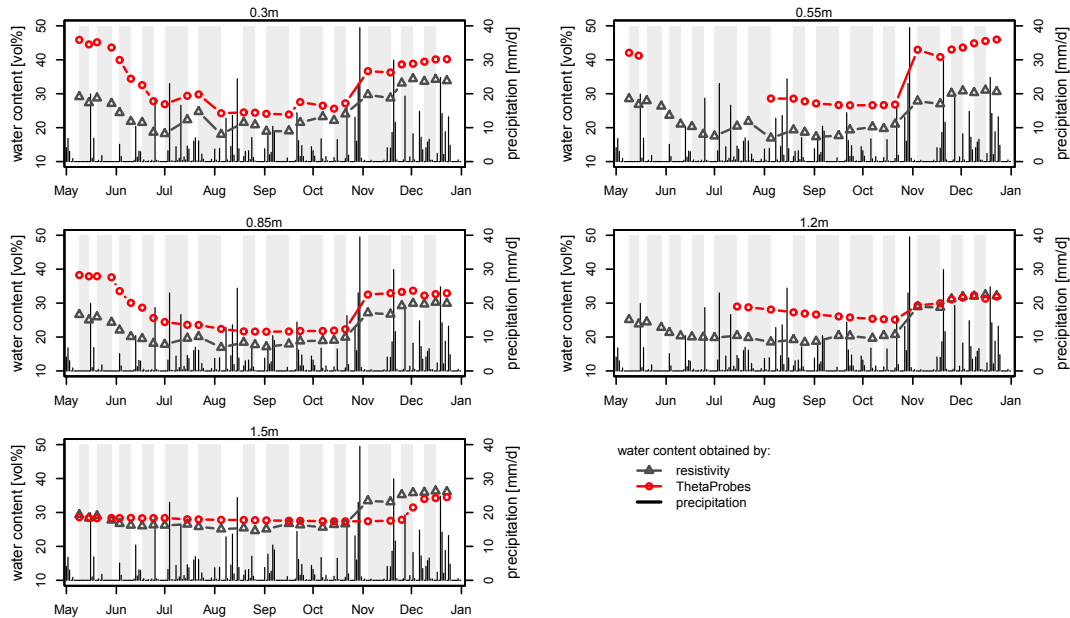
Figure 11. Trend of volumetric water content, obtained by resistivity data and soil moisture sensors (ThetaProbes) with daily precipitation for different depths.

Table 5. Correlation of volumetric water content calculated from resistivity values ($\theta_{\rho H3a}$) and water content from soil moisture sensors (θ_{Theta}) and correlation of resistivity at H3a (ρ_{H3a}) and soil suction at H3a (Ψ_{H3a}).

Depth [m]	$r_{(\theta_{\rho H3a}, \theta_{Theta})}$[a]	$r_{(\rho_{H3a}, \Psi_{H3a})}$
0.30	0.863	0.993[a]
0.55	0.957	0.904[a]
0.85	0.885	0.905[a]
1.20	0.136	0.120[b]
1.50	0.619	0.566[a]

[a] $p < 0.01$; [b] $p > 0.01$.

sensors. In dry periods (e.g. July–October), the difference is less than under humid conditions (e.g. May).

In deeper parts the variations are attenuated. At a depth of 1.2 m there is almost no response over the year, until the heavy rain period at the end of October.

At 1.5 m depth the response of the soil moisture sensor is marginal until December, but thereafter shows an increase. In contrast, $\theta_{\rho H3a}$ shows already in late October a reaction to the heavy rain event, which is not reproducible with the ThetaProbe.

The same holds true for the correlation between resistivity (ρ_{H3a}) and soil suction at H3a (Ψ_{H3a}) (see Table 5). The resistivity of LH and LM fits well to the tensiometer data at the same depth, but in deeper parts it deviates.

These deviations between resistivity data and hydrometric measurements may have different causes. Both methods contain measuring errors, just as the laboratory and other hydrometric (e.g. soil–water resistivity) measurements. Furthermore, the soil moisture sensors and tensiometers measure punctual values. Heller (2012) demonstrated with dye infiltration experiments that preferential flow is an important process in our study area. Hence, hydrometric point measurements may over- or underestimate soil moisture, depending on whether they are inside or outside a preferential pathway. Therefore the data are very limited, with restricted validity for the entire depth range or layer. In contrast, ERT has the advantage of integrating over a larger measuring volume, which makes it more suitable for extensive depth-related interpretations.

4 Conclusions

In drainage basins, hillslopes link precipitation to river runoff. Runoff components, different flow pathways and residence times are mainly influenced by the properties of the hillslope, especially the shallow subsurface. The knowledge of these properties is one of the keys to characterize the runoff dynamics in catchments. According to this, we used ERT for mapping the spatial heterogeneity of the subsurface structure on a hillslope with particular focus on mid-latitude slope deposits (cover beds).

ERT makes it possible to differentiate between LH and LM as one unit and LB as another. Like the intrinsic properties (e.g. sedimentological), LH and LM have very similar electrical characteristics. Therefore, they may only be

distinguished by ERT if water contents are different or change differently with time.

In contrast, the sediments within LB have their own electrical characteristics. The pedo-/petrophysical relationship, with neglecting surface conductivity, shows equal formation factors to LH and LM, but different exponents. With the lower exponent, LB is characterized by lower resistivity at the same water content. Therefore, the resistivity of LB is lower in the entire study area, which is further reinforced by the increasing mineralization of pore water with depth.

From the results of field measurements and pedo-/petrophysical parameter determination in the laboratory we have been able to monitor seasonal changes in subsurface resistivity and its relationship to precipitation and soil moisture on the hillslope scale with a minimally invasive method directly. In combination with commonly used hydrometric approaches, we improved our understanding of the allocation, distribution, and movement of water in the subsurface. Different amounts of precipitation affect the subsurface moisture conditions differently and accordingly different depths take part in runoff generation.

Because pore water (saturation and conductivity) is the main driver for resistivity, we have arrived at some comprehensive interpretations of the subsurface moisture conditions. The high resistivities of LH and LM indicate low water contents, whereas LB is divided into two different moisture zones. On the hillsides water saturation of LB is less than between the depression lines, where low resistivity shows high water saturation and implies a local slope groundwater reservoir.

During the investigation period, temperature-corrected resistivity showed distinct seasonal variations due to changes in moisture conditions, primarily influenced by precipitation and evapotranspiration. Close to the surface, these variations are very evident and decline with increasing depth, mainly limited to a depth of 2 m. This primarily affects LH, LM, and the upper parts of LB, since it may be assumed that deeper parts are already saturated and changes are only possible due to changes in water conductivity.

In summer the subsurface continuously dries, starting at the surface and proceeding to depth. This drying is temporarily interrupted by precipitation. Penetration depth and intensity of the response strongly depend on the amount of precipitation. During periods with a small amount of precipitation, infiltration is limited to LH. There is no runoff generation, and greater depths remain unaffected which leads after repeated occurrence to drier conditions within LM compared to LH. In contrast to this, a response caused by a medium amount of precipitation includes LM and a small increase in spring discharge. The main source of this runoff is saturated overland flow from the surface surrounding the spring. With a high amount of precipitation, changes in resistivity point to vertical seepage down to 2 m. Due to lateral subsurface flow within LH, LM and the upper parts of LB, the discharge of the spring strongly increases.

The results from ERT measurements show a strong correlation to the hydrometric data. The average resistivity response is congruent to the average soil tension data. Water content obtained with soil moisture sensors shows similar variations as calculated from the closest ERT profile. Consequently, soil moisture on the hillslope scale may be determined not only by punctual hydrometric measurements, but also by minimally invasive ERT monitoring, provided pedo-/petrophysical relationships are known. By the use of ERT, expansive invasive hydrometric measurements may be reduced or partially substituted without losing information – but rather enhancing the spatial significance of these conventional point measurements. A combination improves the spatial understanding of the ongoing hydrological processes and is more suitable for the identification of heterogeneities.

Cassiani et al. (2009) pointed out that a combination of geophysical and hydrometric data may be used for quantitative estimation of hillslope moisture conditions. Our study has shown that this may also be applied to mid-latitude hillslopes covered by periglacial slope deposits. Nevertheless, there are some restrictions requiring further improvements.

One shortcoming is the temporal resolution. Some hydrological responses especially at hillslopes may proceed very quickly. The major goal for further research should be to increase the temporal resolution of ERT measurements to at least trace single rain events. This could be realized with automated data acquisitions as described in Kuras et al. (2009).

Another aim should be to improve the spatial resolution. A high-resolution ERT in combination with additional cross-borehole measurements would be more suitable to deal with small-scale heterogeneities and to overcome the problem of decreasing sensitivity with depth.

Edited by: N. Romano

References

AD-hoc AG-Boden: Bodenkundliche Kartieranleitung, 5th Edn., Bundesanst. für Geowiss. und Rohstoffe in Zusammenarb. mit den Staatl. Geol. Diensten, Hannover, 2005.

Amoozegar, A.: A compact constant-head permeameter for measuring saturated hydraulic conductivity of the Vadose Zone, Soil Sci. Soc. Am. J., 53, 1356–1361, 1989.

Anderson, M. G. and Burt, T. P. (Eds.): Process studies in hillslope hydrology, Wiley, Chichester, West Sussex, England, New York, 1990.

Apparao, A.: Geoelectric profiling, Geoexploration, 27, 351–389, 1991.

Archie, G.: The electrical resistivity log as an aid in determining some reservoir characteristics, T. Am. I. Min. Met. Eng., 146, 54–61, 1942.

ATKIS®-DGM2, Landesvermessungsamt Sachsen – Amtliches Topographisch-Kartographische Informationssystem – Digital elevation model, resolution: 2m, 2008

Barker, R.: Depth of investigation of collinear symmetrical four-electrode arrays, Geophysics, 54, 1031–1037, 1989.

Bechtold, M., Vanderborght, J., Weihermueller, L., Herbst, M., Günther, T., Ippisch, O., Kasteel, R., and Vereecken, H.: Up-ward transport in a three-dimensional heterogeneous labora-tory soil under evaporation conditions, Vadose Zone J., 11, doi:10.2136/vzj2011.0066, 2012.

Beff, L., Günther, T., Vandoorne, B., Couvreur, V., and Javaux, M.: Three-dimensional monitoring of soil water content in a maize field using Electrical Resistivity Tomography, Hydrol. Earth Syst. Sci., 17, 595–609, doi:10.5194/hess-17-595-2013, 2013.

Benderitter, Y. and Schott, J. J.: Short time variation of the resis-tivity in an unsaturated soil: the relationship with rainfall, Eur. J. Environ. Eng. Geophys., 4, 37–49, 1999.

Binley, A., Henry-Poulter, S., and Shaw, B.: Examination of solute transport in an undisturbed soil column using electrical resistance tomography, Water Resour. Res., 32, 763–769, 1996a.

Binley, A., Shaw, B., and Henry-Poulter, S.: Flow pathways in porous media: electrical resistance tomography and dye staining image verification, Meas. Sci. Technol., 7, 384–390, 1996b.

Brunet, P., Clément, R., and Bouvier, C.: Monitoring soil water con-tent and deficit using Electrical Resistivity Tomography (ERT) a case study in the Cevennes area, France, J. Hydrol., 48, 146–153, 2010.

Cassiani, G., Bruno, V., Villa, A., Fusi, N., and Binley, A.: A saline trace test monitored via time-lapse surface electrical resistivity tomography, J. Appl. Geophys., 59, 244–259, 2006.

Cassiani, G., Godio, A., Stocco, S., Villa, A., Deiana, R., Frattini, P., and Rossi, M.: Monitoring the hydrologic behaviour of a moun-tain slope via time-lapse electrical resistivity tomography, Near Surf. Geophys., 7, 475–486, 2009.

Chifflard, P., Didszun, J., and Zepp, H.: Skalenübergreifende Prozess-Studien zur Abflussbildung in Gebieten mit periglazialen Deckschichten (Sauerland, Deutschland), Grund-wasser, 13, 27–41, 2008.

Dahlin, T. and Zhou, B.: A numerical comparison of 2-D resistivity imaging with 10 electrode arrays, Geophys. Prospect., 52, 379–398, 2004.

Daily, W., Ramirez, A., LaBrecque, D. J., and Nitao, J.: Electrical resistivity tomography of vadose water movement, Water Resour. Res., 28, 1429–1442, 1992.

De Morais, F., De Almeida Prado Bacellar, L., and Aranha, P. R. A.: Study of flow in vadose zone from electrical resistivity surveys, Rev. Bras. Geofis., 26, 115–122, 2008.

Descloitres, M., Ribolzi, O., and Le Troquer, Y.: Study of infiltra-tion in a Sahelian gully erosion area using time-lapse resistivity mapping, Catena, 53, 229–253, 2003.

Descloitres, M., Ribolzi, O., Troquer, Y. L., and Thiébaux, J. P.: Study of water tension differences in heterogeneous sandy soils using surface ERT, J. Appl. Geophys., 64, 83–98, 2008a.

Descloitres, M., Ruiz, L., Sekhar, M., Legchenko, A., Braun, J., Mo-han Kumar, M. S., and Subramanian, S.: Characterization of sea-sonal local recharge using electrical resistivity tomography and magnetic resonance sounding, Hydrol. Process., 22, 384–394, 2008b.

Di Baldassarre, G. and Uhlenbrook, S.: Is the current flood of data enough? A treatise on research needs for the improvement of flood modelling, Hydrol. Process., 26, 153–158, 2012.

French, H. and Binley, A.: Snowmelt infiltration: monitoring tempo-ral and spatial variability using time-lapse electrical resistivity, J. Hydrol., 297, 174–186, 2004.

Garré, S., Koestel, J., Günther, T., Javaux, M., Vanderborght, J., and Vereecken, H.: Comparison of heterogeneous transport processes observed with electrical resistivity tomography in two soils, Va-dose Zone J., 9, 336–349, 2010.

Garré, S., Javaux, M., Vanderborght, J., Pages, L., and Vereecken, H.: Three-dimensional electrical resistivity to-mography to monitor root zone water dynamics, Vadose Zone J., 10, 412–424, 2011.

Günther, T., Rücker, C., and Spitzer, K.: Three-dimensional mod-elling and inversion of dc resistivity data incorporating topogra-phy – II. Inversion, Geophys. J. Int., 166, 506–517, 2006.

Hayashi, M.: Temperature-electrical conductivity relation of wa-ter for environmental monitoring and geophysical data inversion, Environ. Monit. Assess., 96, 119–128, 2004.

Heller, K.: Einfluss periglazialer Deckschichten auf die ober-flächennahen Fließwege am Hang – eine Prozessstudie im Os-terzgebirge, Sachsen, Ph.D. thesis, Faculty of Environmental Sciences, TU Dresden, available at: http://nbn-resolving.de/urn: nbn:de:bsz:14-qucosa-98437 (last access: 30 April 2014), 2012.

Keller, G. V. and Frischknecht, F. C.: Electrical Methods in Geo-physical Prospecting, Pergamon Press, Oxford, 1966.

Kemna, A., Vanderborght, J., Hardelauf, H., and Vereecken, H.: Quantitative imaging of 3-D solute transport using 2-D time-lapse ERT: a synthetic feasibility study, in: 17th EEGS Sympo-sium on the Application of Geophysics to Engineering and Envi-ronmental Problems, Colorado, USA, 342–353, 2004.

Kirkby, M. J. (Ed.): Hillslope Hydrology, Wiley, Chichester, 1980.

Kleber, A.: Lateraler Wasserfluss in Hangsedimenten unter Wald, in: Stoff- und Wasserhaushalt in Einzugsgebieten, Beiträge zur EU-Wasserrahmenrichtlinie, edited by: Lorz, C. and Haase, D., Springer Verlag, Heidelberg, 7–22, 2004.

Kleber, A. and Schellenberger, A.: Slope hydrology triggered by cover-beds, With an example from the Frankenwald Mountains, northeastern Bavaria, Z. Geomorphol., 42, 469–482, 1998.

Kleber, A. and Terhorst, B. (Eds.): Mid-Latitude Slope Deposits (Cover Beds), vol. 66 of Developments in sedimentology, 1st Edn., Elsevier, Amsterdam, Boston, Heidelberg, London, New York, Oxford, Paris, San Diego, San Francisco, Singapore, Sydney, Tokyo, 2013.

Klute, A. (Ed.): Methods of Soil Analysis, Part 1: Physical and Min-eralogical Methods, 2nd Edn., ASA, SSA, Madison, Wisconsin, 1986.

Koestel, J., Kemna, A., Javaux, M., Binley, A., and Vereecken, H.: Quantitative imaging of solute transport in an unsaturated and undisturbed soil monolith with 3-D ERT and TDR, Water Resour. Res., 44, W12411, doi:10.1029/2007WR006755, 2008.

Koestel, J., Vanderborght, J., Javaux, M., Kemna, A., Binley, A., and Vereecken, H.: Noninvasive 3-D transport characterization in a sandy soil using ERT: 1. Investigating the validity of ERT-derived transport parameters, Vadose Zone J., 8, 711–722, 2009a.

Koestel, J., Vanderborght, J., Javaux, M., Kemna, A., Binley, A., and Vereecken, H.: Noninvasive 3-D transport characterization in a sandy soil using ERT: 2. Transport process inference, Vadose Zone J., 8, 723–734, 2009b.

Kuras, O., Pritchard, J. D., Meldrum, P. I., Chambers, J. E., Wilkinson, P. B., Ogilvy, R. D., and Wealthall, G. P.: Monitoring hydraulic processes with automated time-lapse electrical resistivity tomography (ALERT), CR Geosci., 341, 868–885, 2009.

LaBrecque, D. J., Miletto, M., Daily, W., Ramirez, A., and Owen, E.: The effects of noise on Occam's inversion of resistivity tomography data, Geophysics, 61, 538–548, 1996.

Leslie, I. N. and Heinse, R.: Characterizing soil-pipe networks with pseudo-three-dimensional resistivity tomography on forested hillslopes with restrictive horizons, Vadose Zone J., 12, doi:10.2136/vzj2012.0200, 2013.

Lesmes, D. P. and Friedman, S. P.: Relationships between the electrical and hydrogeological properties of rocks and soils, in: Hydrogeophysics, edited by: Rubin, Y. and Hubbard, S. S., Springer, Dordrecht, 87–128, 2006.

Ma, R., McBratney, A., Whelan, B., Minasny, B., and Short, M.: Comparing temperature correction models for soil electrical conductivity measurement, Precis. Agric., 12, 55–66, 2011.

Massuel, S., Favreau, G., Descloitres, M., Le Troquer, Y., Albouy, Y., and Cappelaere, B.: Deep infiltration through a sandy alluvial fan in semiarid Niger inferred from electrical conductivity survey, vadose zone chemistry and hydrological modelling, Catena, 67, 105–118, 2006.

McDonnell, J. J.: Where does water go when it rains? Moving beyond the variable source area concept of rainfall–runoff response, Hydrol. Process., 17, 1869–1875, 2003.

McDonnell, J. J., Tanaka, T., Mitchell, M. J., and Ohte, N.: Hydrology and biogeochemistry of forested catchments, Hydrol. Process., 15, 1673–1674, 2001.

McDonnell, J. J., Sivapalan, M., Vaché, K., Dunn, S., Grant, G., Haggerty, R., Hinz, C., Hooper, R., Kirchner, J., Roderick, M. L., Selker, J., and Weiler, M.: Moving beyond heterogeneity and process complexity: a new vision for watershed hydrology, Water Resour. Res., 43, W07301, doi:10.1029/2006WR005467, 2007.

Michot, D., Benderitter, Y., Dorigny, A., Nicoullaud, B., King, D., and Tabbagh, A.: Spatial and temporal monitoring of soil water content with an irrigated corn crop cover using surface electrical resistivity tomography, Water Resour. Res., 39, SBH 14-1–SBH 14-20, 2003.

Miller, C. R., Routh, P. S., Brosten, T. R., and McNamara, J. P.: Application of time-lapse ERT imaging to watershed characterization, Geophysics, 73, G7–G17, 2008.

Moldenhauer, K.-M., Heller, K., Chifflard, P., Hübner, R., and Kleber, A.: Influence of cover beds on slope hydrology, in: Mid-Latitude Slope Deposits (Cover Beds), edited by: Kleber, A. and Terhorst, B., vol. 66 of Developments in Sedimentology, Elsevier, Amsterdam etc., 127–152, 2013.

Oldenborger, G. A., Knoll, M. D., Routh, P. S., and LaBrecque, D. J.: Time-lapse ERT monitoring of an injection/withdrawal experiment in a shallow unconfined aquifer, Geophysics, 72, F177–F188, 2007.

Perri, M. T., Cassiani, G., Gervasio, I., Deiana, R., and Binley, A.: A saline tracer test monitored via both surface and cross-borehole electrical resistivity tomography: comparison of time-lapse results, J. Appl. Geophys., 79, 6–16, 2012.

Popp, S., Altdorff, D., and Dietrich, P.: Assessment of shallow subsurface characterisation with non-invasive geophysical methods at the intermediate hill-slope scale, Hydrol. Earth Syst. Sci., 17, 1297–1307, doi:10.5194/hess-17-1297-2013, 2013.

Ramirez, A., Daily, W., LaBrecque, D. J., Owen, E., and Chesnut, D.: Monitoring an underground steam injection process using electrical resistance tomography, Water Resour. Res., 29, 73–87, 1993.

Robinson, D. A., Binley, A., Crook, N., Day-Lewis, F. D., Ferré, T. P. A., Grauch, V. J. S., Knight, R., Knoll, M. D., Lakshmi, V., Miller, R., Nyquist, J., Pellerin, L., Singha, K., and Slater, L.: Advancing process-based watershed hydrological research using near-surface geophysics: a vision for, and review of, electrical and magnetic geophysical methods, Hydrol. Process., 22, 3604–3635, 2008a.

Robinson, D. A., Campbell, C. S., Hopmans, J. W., Hornbuckle, B. K., Jones, S. B., Knight, R., Ogden, F., Selker, J., and Wendroth, O.: Soil moisture measurement for ecological and hydrological watershed-scale observatories: a review, Vadose Zone J., 7, 358–389, 2008b.

Robinson, D. A., Abdu, H., Lebron, I., and Jones, S. B.: Imaging of hill-slope soil moisture wetting patterns in a semi-arid oak savanna catchment using time-lapse electromagnetic induction, J. Hydrol., 416, 39–49, 2012.

Roy, A. and Apparao, A.: Depth of investigation in direct current methods, Geophysics, 36, 943–959, 1971.

Rücker, C. and Günther, T.: The simulation of Finite ERT electrodes using the complete electrode model, Geophysics, 76(4), F227–238, 2011.

Sauer, D., Scholten, T., and Felix-Henningsen, P.: Verbreitung und Eigenschaften periglaziärer Lagen im östlichen Westerwald in Abhängigkeit von Gestein, Exposition und Relief, Mitt. Dtsch. Bodenkdl. Ges., 96, 551–552, 2001.

Scholten, T.: Periglaziäre Lagen in Mittelgebirgslandschaften – Verbreitungssystematik, Eigenschaften und Bedeutung für den Landschaftswasser- und stoffhaushalt, in: Tagungsbeiträge IFZ-Workshop Ressourcensicherung in der Kulturlandschaft, Selbstverlag, Justus-Liebig-Universität, Gießen, 11–15, 1999.

Schön, J. H.: Physical Properties of Rocks: Fundamentals and Principles of Petrophysics, vol. 18 of Handbook of Geophysical Exploration: Seismic Exploration, Elsevier, Oxford, 2004.

Singha, K. and Gorelick, S. M.: Saline tracer visualized with three-dimensional electrical resistivity tomography: field-scale spatial moment analysis, Water Resour. Res., 41, W05023, doi:10.1029/2004WR003460, 2005.

Slater, L., Binley, A., Daily, W., and Johnson, R.: Cross-hole electrical imaging of a controlled saline tracer injection, J. Appl. Geophys., 44, 85–102, 2000.

Tilch, N., Uhlenbrook, S., Didszun, J., Wenninger, J., Kirnbauer, R., Zillgens, B., and Leibundgut, C.: Hydrologische Prozessforschung zur Hochwasserentstehung im Löhnersbach-Einzugsgebiet (Kitzbüheler Alpen, Österreich), Hydrol. Wasserbewirts., 50, 67–78, 2006.

Tromp-van Meerveld, H. J.: Hillslope hydrology: from patterns to processes, Ph.D. thesis, Oregon State University, Corvallis, 2004.

Tromp-van Meerveld, H. J. and McDonnell, J. J.: Assessment of multi-frequency electromagnetic induction for determining soil moisture patterns at the hillslope scale, J. Hydrol., 368, 56–67, 2009.

Uchida, T., McDonnell, J. J., and Asano, Y.: Functional intercomparison of hillslopes and small catchments by examining water source, flowpath and mean residence time, J. Hydrol., 327, 627–642, 2006.

Uhlenbrook, S.: Von der Abflussbildungsforschung zur prozessorientierten Modellierung – ein Review, Hydrol. Wasserbewirts., 49, 13–24, 2005.

Uhlenbrook, S., Didszun, J., and Wenninger, J.: Source areas and mixing of runoff components at the hillslope scale – a multi-technical approach, Hydrolog. Sci. J., 53, 741–753, 2008.

Vanderborght, J., Kemna, A., Hardelauf, H., and Vereecken, H.: Potential of electrical resistivity tomography to infer aquifer transport characteristics from tracer studies: a synthetic case study, Water Resour. Res., 41, W06013, doi:10.1029/2004WR003774, 2005.

Völkel, J., Leopold, M., Mahr, A., and Raab, T.: Zur Bedeutung kaltzeitlicher Hangsedimente in zentraleuropäischen Mittelgebirgslandschaften und zu Fragen ihrer Terminologie, Petermann. Geogr. Mitt., 146, 50–59, 2002a.

Völkel, J., Zepp, H., and Kleber, A.: Periglaziale Deckschichten in Mittelgebirgen – ein offenes Forschungsfeld, Ber. deuts. Landesk., 76, 101–114, 2002b.

Wenninger, J., Uhlenbrook, S., Tilch, N., and Leibundgut, C.: Experimental evidence of fast groundwater responses in a hillslope/floodplain area in the Black Forest Mountains, Germany, Hydrol. Process., 18, 3305–3322, 2004.

Zhou, B. and Dahlin, T.: Properties and effects of measurement errors on 2-D resistivity imaging surveying, Near Surf. Geophys., 1, 105–117, 2003.

Zhou, Q. Y., Shimada, J., and Sato, A.: Three-dimensional spatial and temporal monitoring of soil water content using electrical resistivity tomography, Water Resour. Res., 37, 273–285, 2001.